Timescales of quantum and classical chaotic spin models evolving toward equilibrium

Fausto Borgonovi,[1,2] Felix M. Izrailev,[3,4] and Lea F. Santos[5]

[1] *Dipartimento di Matematica e Fisica and Interdisciplinary Laboratories for Advanced Materials Physics, Università Cattolica, via della Garzetta 48, 25133 Brescia, Italy*
[2] *Istituto Nazionale di Fisica Nucleare, Sezione di Milano, via Celoria 16, I-20133, Milano, Italy*
[3] *Instituto de Física, Benemérita Universidad Autónoma de Puebla, Apartado Postal J-48, Puebla 72570, Mexico*
[4] *Department of Physics and Astronomy, Michigan State University, E. Lansing, Michigan 48824-1321, USA*
[5] *Department of Physics, University of Connecticut, Storrs, Connecticut 06269, USA*

We investigate the quench dynamics of a one-dimensional strongly chaotic lattice with L interacting spins. By analyzing both the classical and quantum dynamics, we identify and elucidate the two mechanisms of the relaxation process of this systems: one arises from linear parametric instability and the other from nonlinearity. We demonstrate that the relaxation of the single-particles energies (global quantity) and of the onsite magnetization (local observable) is primarily due to the first mechanism, referred to as linear chaos. Our analytical findings indicate that both quantities, in the classical and quantum domain, relax at the same timescale, which is independent of the system size. The physical explanation for this behavior lies in the fact that each spin is constrained to the surface of a three-dimensional unit sphere, instead of filling the whole many-dimensional phase space. We argue that observables with a well-defined classical limit should conform to this picture and exhibit a finite relaxation time in the thermodynamic limit. In contrast, the evolution of the participation ratio, which measures how the initial state spreads in the many-body Hilbert space and has no classical limit, indicates absence of relaxation in the thermodynamic limit.

I. INTRODUCTION

Much attention has recently been devoted to the relaxation process of isolated many-body quantum systems toward statistical equilibrium and how their relaxation time depends on model parameters. Different investigations have yielded contradictory conclusions with respect to the dependence of the relaxation time on the system size L: some suggest that it decreases with L [1, 2], depends weakly on L [3, 4], does not depend on L [5], or increases with L [1, 6–17] either polynomially or exponentially, depending on the observable [18]. The problem remains open due to the absence of a general theoretical framework and the inherent difficulty in simulating quantum systems with a large number of particles.

Recently, we proposed a new approach [19] for describing the statistical properties of interacting many-body quantum systems with a well-defined classical limit. The premise is that, under the condition of strong chaos in both the quantum and classical models, some global characteristics of the eigenstates can be derived from the classical equations of motion. Given that the theoretical analysis of classical systems is relatively simpler than that of quantum systems, one can readily obtain semi-analytical results based on the properties of classical chaos and apply them to the quantum systems. In Ref. [19], we demonstrated the effectiveness of this approach using a one-dimensional (1D) spin model with varying short-range interactions. Through detailed numerical analyses, we showed that quantities that serve as building blocks of physical observables coincide in the classical and quantum descriptions. One such quantity is the local density of states (LDoS).

The LDoS determines the energy distribution of the initial state in quench dynamics. In nuclear physics, it is known as strength function and is used to study the scattering properties of particles in nuclear reactions [20]. The width of the quantum LDoS characterizes the growth rate of the participation ratio, that is of the number of many-body states participating in the evolution of an initially excited state [21, 22], and the absolute square of the Fourier transform of the LDoS is the survival probability of the initial state. As detailed in [19], in cases where the system exhibits a well-defined classical limit, the LDoS can be obtained from the classical trajectories associated with the non-interacting Hamiltonian H_0 by projecting them onto the total Hamiltonian $H = H_0 + V$, where V represents the inter-particle interaction. The classical LDoS coincides with the quantum one when the system is strongly chaotic even for small quantum number.

The goal of the present paper is to investigate the quantum-classical correspondence (QCC) for many-body systems out of equilibrium. This is challenging, because the phase space of classical many-body models is multidimensional and the Hilbert space of the quantum many-body models grows exponentially with the number of spins, which makes the QCC analysis nearly intractable. Recent studies in this direction have been done in the context of the out-of-time-ordered correlator [23, 24], and have involved spin models [25–27] and a p-spin glass model [28], though numerous questions remain open. Our approach is inspired by the QCC established for many-body spin models in [19], which we now explore for the analysis of the dynamical properties of those systems. The focus is on the different timescales identified along the relaxation process of various observables. With our approach, we can use the classical model to obtain semi-analytical expressions that successfully describe the quantum evolution.

Our study concentrates on the classical and quantum

evolution toward equilibrium of both global and local observables, aiming at estimating their relaxation time. Specifically, we consider a 1D model of L interacting spins in the chaotic regime and investigate the evolution of the energy associated with the non-interacting Hamiltonian, which is a global quantity, and of the onsite magnetization, which is a local quantity. Our numerical results and analytical estimates reveal that the evolution of the energy variance shows excellent QCC and increases linearly over time, which indicates a diffusive-like spreading.

Due to the strong chaos and ergodicity of the classical motion of the individual spins on 3D spheres, the energy spread leads to the ergodic filling of the energy shell. Surprisingly, we find that the timescale for the diffusive spread of energy is independent of the number of spins. The same holds for the relaxation time of the magnetization of individual spins. We attribute this result to both the fact that each spin is constrained to the surface of a 3D unit sphere, leading to the existence of L local integrals of motion, and to choice of uncorrelated single particles frequencies. The latter condition leads to the linear dependence of the frequencies variance on the system size L, which results in the system-size-independence of the relaxation time. We argue that, in this system, classical chaos is primarily caused by linear parametric instability rather than by the interaction between nonlinear resonances.

We also investigate the evolution of the participation ratio (aka number of principal components), $P_R(t)$. In contrast to the energy and magnetization, $P_R(t)$ does not have a classical limit. This quantity measures the number of many-body states that characterize the spread of the initial state in the Hilbert space, being thus equivalent to the exponential of a participation entropy. Our numerical data confirm that $P_R(t)$ exhibits an exponential growth over time, with a rate determined by the width of the LDoS, and demonstrate that this quantity eventually reaches saturation at a time that grows with the number of spins L. This observation aligns with existing results for interacting fermions and bosons [21, 29]. Our analytical analysis shows that the relaxation time is proportional to $\sqrt{L}$. This means that the dynamics of the participation ratio does not saturate in the thermodynamic limit ($L \to \infty$), which means that thermalization defined in terms of this quantity does not occur in the thermodynamic limit.

The paper is organized as follows. In Sec. II, we describe the spin model in the quantum and classical domain. In Sec. III, we analyze the quantum and classical spread of the single-particles energies, identifying the timescales for ballistic and diffusive behaviors before saturation, and comparing the diffusion time with the Lyapunov time. In Sec. IV, we study the dynamics of the magnetization in the z-direction of individual spins and find agreement with the timescales for the energy spreading. In Sec. V, we clarify the concept of linear chaos and how it helps to explain why the relaxation time for energy and magnetization does not depend on the system size. In Sec. VI, we investigate the evolution of the participation ration, which has no classical limit and whose relaxation time does depend on system size. Conclusions are provided in Sec. VII.

II. QUANTUM AND CLASSICAL MODEL

We consider the same model explored in Ref. [19]. The total Hamiltonian of the model,

$$H = H_0 + V, \tag{1}$$

consists of two parts.

The first part,

$$H_0 = \sum_{k=1}^{L} B_k S_k^z, \tag{2}$$

describes L non-interacting spins on a 1D lattice in a slightly inhomogeneous magnetic field along the z-axis. B_k are the local frequencies associated with each spin. We consider an almost homogeneous distribution of the single-particle frequencies $B_k = B_0 + \delta B_k$, where $B_0 = 1$ and δB_k are small random entries, $|\delta B_k| \leq \delta W \ll B_0$. However, we show in Sec. IV that this particular choice does not affect the generality of our results, provided classical chaos is strong enough to guarantee the ergodicity of the motion of the single spins on their individual 3D-unit spheres.

The second part of the total Hamiltonian,

$$V = J_0 \sum_{k=1}^{L-1} \sum_{i=k+1}^{L} \frac{1}{|i-k|^\nu} S_i^x S_k^x, \tag{3}$$

describes the spins interaction. They are subjected to a two-body interaction V of strength J_0 and a variable interaction range determined by ν. We set $J_0 > B_0$, which guarantees strong chaos [19] both in the quantum and classical descriptions. In what follows, we mostly consider $\nu = 1.4$, which corresponds to short-range interaction and is also referred to as "weak long-range" interaction [30]. Additional results for different ranges $\nu > 1$ are also provided in Sec. IV and show that the outcomes are independent of ν in the short-range regime.

A. Quantum Model

The spins are quantized with an integer value S and the effective Planck constant is $\hbar = 1/\sqrt{S(S+1)}$, so that the semiclassical limit is achieved for $S \gg 1$. The "non-interacting many-body basis" (in which H_0 is a diagonal matrix) corresponds to the eigenstates of H_0 and is denoted by $|k\rangle \equiv |s_1, ..., s_j, ..., s_L\rangle$, where $-S \leq s_j \leq S$ and $j = 1, ..., L$. The interaction V couples basis vectors that differ by two excitations, so there are two symmetry sectors, each of dimension $\dim = (2S+1)^L/2$.

Quantum initial state: The quantum dynamics starts after a quench from H_0 to H, so that the initial state

$|\Psi(0)\rangle$ is a many-body basis vector $|k_0\rangle$. The components of the evolving wave function at time t, written in the many-body noninteracting basis, are

$$\langle k|\Psi(t)\rangle = \sum_\alpha C_k^\alpha \left(C_{k_0}^\alpha\right)^* e^{-iE_\alpha t/\hbar}, \tag{4}$$

where

$$C_k^\alpha \equiv \langle k|\alpha\rangle \tag{5}$$

and $|\alpha\rangle$ is an eigenstate of the total Hamiltonian H with energy E_α. We consider initial states with energy in the middle of the spectrum, $E_0 = \langle\Psi(0)|H|\Psi(0)\rangle \simeq 0$, where the system has been found to be maximally chaotic [19].

B. Classical Model

The starting point for the classical model are the classical equations of motion,

$$\begin{aligned} \dot{S}_k^x &= -B_k S_k^y, \\ \dot{S}_k^y &= B_k S_k^x + S_k^z \sum_{i\neq k} J_{ik} S_i^x, \\ \dot{S}_k^z &= -S_k^y \sum_{i\neq k} J_{ik} S_i^x, \end{aligned} \tag{6}$$

which automatically guarantee the conservation of the angular momentum $|\vec{S}_k|^2 = 1$ for each k.

The motion of each spin occurs onto a 3D unit sphere, as explained in [19]. However, the motion of S_x and S_y is principally different from that of S_z. If the interaction is very weak, the k-th spin rotates around the z-axis with frequency B_k, keeping the S_z-component almost constant. In contrast, if the interaction is strong, one expects the full coverage of the unit sphere. An important question is then how the chaotic properties of the motion of individual spins emerge with the increase of the spin-spin interaction. The detailed analysis performed in [19] revealed the following.

Since the trajectory of any spin is confined to the unit sphere, the instability of the motion is defined simply by the maximal positive Lyapunov exponent associated with the motion of a single spin, λ_+. The value of λ_+ can be found numerically from the second-order differential equation for S_k^z obtained from Eq. (6),

$$\ddot{S}_z^k + \Omega_k^2(t) S_z^k = F_k(t), \tag{7}$$

where both

$$\Omega_k^2(t) = J_0^2 \left[\sum_{j\neq k} \frac{S_j^x(t)}{|j-k|^\nu}\right]^2, \tag{8}$$

$$F_k(t) = J_0 \sum_{j\neq k} \frac{B_j S_j^y(t) S_k^y(t) - B_k S_j^x(t) S_k^x(t)}{|j-k|^\nu} \tag{9}$$

are quasi-periodic functions defined by the motion of all other spins. In first-order of perturbation theory (in J_0) the two functions above do not depend on the S_z^k-component. This means that the motion in Eq. (7) is described by a linear parametric oscillator with an external quasi-periodic force with many frequencies originated from the set of unperturbed frequencies B_k. Thus, for a relatively weak perturbation J_0, the mechanism of chaos is the same known to emerge in linear time-dependent models. The analysis shows that the effect of non-linearity, which is a common mechanism of classical chaos, occurs in the next order approximation. As one sees, the instability of the spin-motion is due to both linear and non-linear mechanisms, but the latter plays a minor role in the short-time relaxation of the system, as will be clear below.

Note that the instability of the motion of the individual spins can be measured numerically in a relatively easy way, in contrast with the very difficult procedure of finding the Lyapunov spectra. Our numerical analysis in [19] has shown that the maximal Lyapunov exponent associated with the motion of a single spin, λ_+, approximately equals the maximal Lyapunov exponent in the total spectrum of exponents of the many-body spin model. This significantly simplifies the derivation of the characteristic timescale defined by the Lyapunov spectra [31].

Since local instability determined by the Lyapunov exponent is not enough to characterize global chaos, which is typically associated with ergodicity, we carefully analyzed the problem of classical ergodicity in Ref. [19]. As explained there, a very efficient and simple way to rigorously define classical ergodicity in spin systems is to verify the ergodicity of the motion of each individual spin on its unit sphere. This significantly simplifies the numerical analysis of ergodicity, because we do not need to consider the full many-dimensional phase space. Specifically, in [19], we proved the single spin ergodicity by (i) finding the distribution of each one of the three Cartesian components of each single spin, $S_x(t)$, $S_y(t)$, and $S_z(t)$, and (ii) showing that these distributions follow the expression for each component of the random eigenstates of 3D random matrices. In this way, we numerically obtained that our model is completely ergodic and chaotic for $J_0 \gtrsim 3$. This value marks the crossover from a partially chaotic to an ergodic system with strong chaos both in the quantum and classical description.

Classical initial conditions: To keep the quantum-classical description as close as possible, we choose a set of classical initial conditions where $S_k^z(0)$ is such that $H_0(0) = \sum_k B_k S_k^z(0) = 0$ and $S_k^{x,y}(0)$ are randomly chosen in $[-1, 1]$. This is the classical analogue to the quantum initial state where the values for the spins in the z-direction are fixed, so $\langle S_k^x\rangle = \langle S_k^y\rangle = 0$, and $E_0 \simeq 0$.

III. RELAXATION IN THE ENERGY SHELL: GLOBAL OBSERVABLE

Our goal in this paper is to establish, both semi-analytically and numerically, the timescales that characterize the quantum evolution after a quench toward equilibrium and how they depend on the parameters of

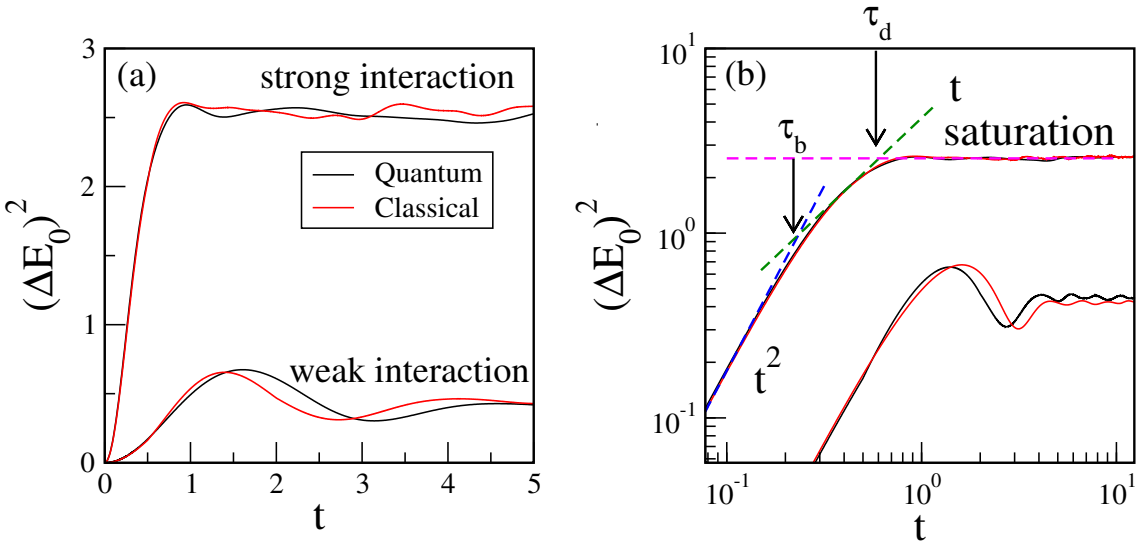

FIG. 1. (a) Classical and quantum energy spread $(\Delta E_0)^2(t)$ in time for two interaction strengths: strong interaction $J_0 = 3$ (upper curves) and weak interaction $J_0 = 0.6$ (lower curves). Red curves correspond to the classical data and black curves, to quantum data. (b) Same as (a) but in the log-log scale to better show the different behaviors at different timescales. Dashed blue line indicates ballistic behavior $(\Delta E_0)^2 \propto t^2$, dashed green lines indicates diffusive behavior $(\Delta E_0)^2 \propto t$, and the saturation of the dynamics $(\Delta E_0)^2 \propto const$ is marked with the horizontal dashed magenta line. The vertical arrows indicate the approximate values of τ_b, where the behavior changes from ballistic to diffusive, and τ_d, where the diffusive dynamics saturates. The parameters are: $L = 9$, $B_0 = 1$, $\delta W = 0.2$, $\nu = 1.4$. For the classical case, the average is done over $10^4/L$ initial conditions with $|E_0| < 0.01$. For the quantum case, the average is done over 50 initial basis states with energy $|E_0| < 0.01$. For the quantum simulation, we use the spin quantum number $S = 1$.

our spin model. To this end, we compare the quantum and classical dynamics of a global observable in this section and of a local observable in the next section. The analysis of the evolution of a quantity that has no classical limit is left for Sec. VI.

In both the quantum and the classical model, the dynamics takes place in the energy shell, which is defined by the projection of H onto H_0 [19]. The width of the shell is restricted by the strength of inter-particle interaction, not by the whole energy space.

The global observable that we consider in this section is the variance of the energies of the single particles given by H_0. This quantity spreads in the energy shell due to the inter-particle interaction. In the quantum model, it is defined by the following relation

$$(\Delta E_0)^2(t) = \langle\Psi(t)|H_0^2|\Psi(t)\rangle - \langle\Psi(t)|H_0|\Psi(t)\rangle^2. \quad (10)$$

The corresponding classical quantity is obtained by substituting the quantum average $\langle ...\rangle$ with the average over many initial conditions (see Sec. II B), indicated as $\overline{(\dots)}$.

Notice that in the quantum case, the energy of the initial state, which is an eigenstate of H_0, can be equivalently computed in terms of the total Hamiltonian or in terms of the noninteracting Hamiltonian,

$$E_0 = \langle\Psi(0)|H|\Psi(0)\rangle = \langle\Psi(0)|H_0|\Psi(0)\rangle, \quad (11)$$

because the two-body interaction between spins has zero diagonal matrix elements in the basis of H_0.

To identify the different timescales emerging during the dynamical process, let us first compare in Fig. 1 the classical and quantum results for $(\Delta E_0)^2(t)$ numerically obtained for two interaction strengths, weak ($J_0 = 0.6$) and strong ($J_0 = 3$) interaction. The spin quantum number considered is $S = 1$. One sees that the correspondence between the quantum and classical results is extremely good even for such small spin number.

The curve for strong interaction ($J_0 = 3$) in Fig. 1(b) exhibits three different dynamical regimes. The dynamics is initially ballistic (blue dashed line), then it becomes diffusive (green dashed line), before finally relaxing to equilibrium (magenta dashed line). On the other hand, the diffusive regime is absent for weak interaction ($J_0 = 0.6$), so saturation happens after the ballistic spread. In Ref. [19], it was numerically proved that for strong interaction, the motion is not only chaotic (defined by a maximal positive Lyapunov exponent), but also ergodic on the unit sphere of each spin. In contrast, for weak interaction, where diffusion is absent, the dynamics is not ergodic, even though the presence of a maximal positive Lyapunov exponent signals the presence of classical chaos. Despite these differences, we observe in Fig. 1, that the QCC occurs independently of the interaction strength and over all timescales, ballistic, diffusive, and stationary.

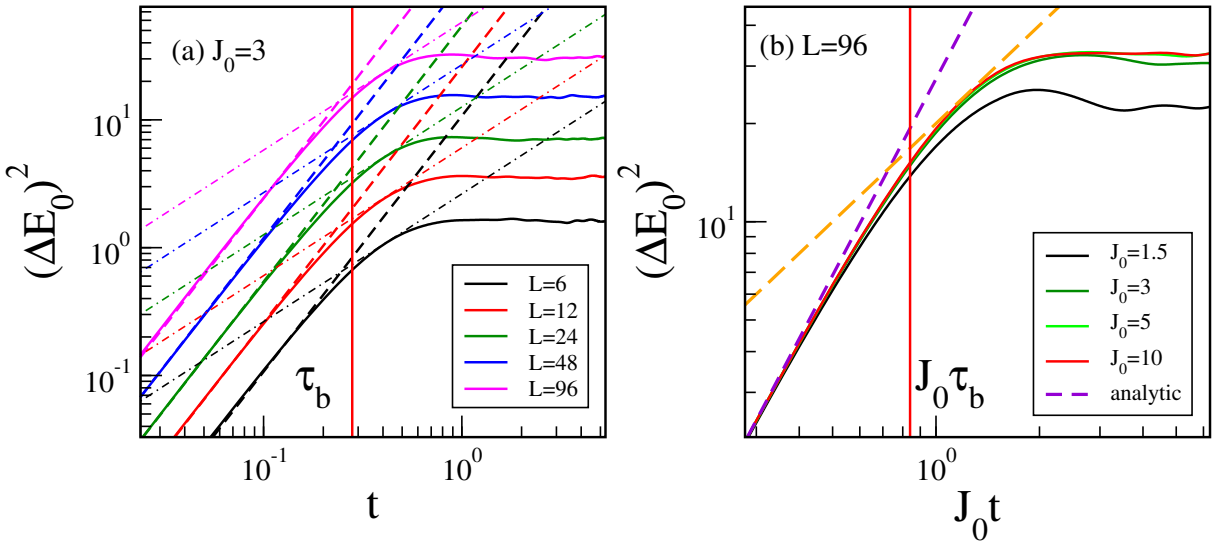

FIG. 2. (a) Classical energy spread in time, $(\Delta E_0)^2(t)$, for a strong interaction strength, $J_0 = 3$, and different number of spins L, as indicated in the legend. Dashed and dot-dashed lines indicate, respectively, the ballistic and the diffusive behavior. The dashed vertical line marks the time τ_b in Eq. (21) at which the dynamics switches from ballistic to diffusive, thus demonstrating the independence on L for this timescale. (b) Classical energy spread as a function of $J_0 t$ for $L = 96$ and different values of J_0. The curves collapse on each other and the intersection between the ballistic and diffusive regimes is a single point $J_0\tau_b = const$, thus indicating that $\tau_b \propto 1/J_0$. The purple dashed line corresponds to Eq. (13), obtained for the ballistic behavior at short times in the limit of large system size. The orange dashed line indicates the diffusive behavior and is obtained using Eq. (19). The vertical solid line corresponds to Eq. (21). The average was performed over $10^4/L$ initial conditions with $|E_0| < 0.01$. The other parameters are $B_0 = 1, \delta W = 0.2, \nu = 1.4$.

A. Ballistic regime

In this subsection, we perform a semi-analytical study of the shortest timescale, which is characterized by ballistic propagation. We turn to the classical model to derive analytical estimates, which are then compared with numerical data.

For short time, the variance $(\Delta E_0)^2(t)$ is proportional to t^2. To find the time τ_b at which the spreading of energy switches from ballistic to diffusive, we first need to find the velocity v_b defined by the equation $\Delta E_0 = v_b t$. This, in turn, can be obtained from the classical equations of motion by expanding $S_k^z(t)$ for short time,

$$S_k^z(t) = S_k^z(0) + t\dot{S}_k^z(0) + (1/2)t^2\ddot{S}_k^z(0) + O(t^3)$$

and taking into account that we choose initial conditions to have $E_0(0) = 0$. As mentioned before, this means that the z-component of all spins, $S_k^z(0)$, initially leads to $\sum_k B_k S_k^z(0) = 0$ and the x and y components are chosen to be completely random (keeping fixed the unit length for the spin vector).

Taking the ensemble average over the initial random conditions and using Eq. (6), we can show that

$$\begin{aligned}(\Delta E_0)^2(t) &= t^2\overline{\left(\sum_{k=1}^{L} B_k \sum_{j\neq k} J_{k,j} S_k^y(0) S_j^x(0)\right)^2} + O(t^3) \\ &= \frac{t^2}{9}\left(\sum_{k=1}^{L} B_k^2 \sum_{j\neq k} J_{k,j}^2\right) + O(t^3), \end{aligned} \tag{12}$$

where the last equality is due to our choice of completely random x and y components, so that the nonzero terms are $\overline{S_k^y(0)^2} = \overline{S_j^x(0)^2} = 1/3$. The analytical expression in Eq. (12) is plotted in Fig. 2(a) (dashed lines) and compared with numerical results (full curves) for different system sizes L and a strong interaction strength that guarantees the ergodic motion. We reiterate that the dashed lines characterizing the short-time dynamics are not fitting lines, but correspond to Eq. (12).

In the limit of large system size, Eq. (12) can be further simplified as

$$\begin{aligned}(\Delta E_0)^2(t) \equiv v_b^2 t^2 &= \left(\sum_{k=1}^{L} B_k^2 \sum_{j\neq k} J_{k,j}^2\right)\frac{t^2}{9} \\ &\simeq \frac{2}{9}\sum_{k=1}^{L} B_k^2 J_0^2 \sum_{j=1}^{\infty}\frac{1}{j^{2\nu}} t^2 \simeq \frac{2}{9} L\langle B^2\rangle J_0^2 \zeta(2\nu) t^2, \end{aligned} \tag{13}$$

where in the last equality, we defined implicitly the Riemann zeta function $\zeta(2\nu)$, which is finite for $\nu > 1/2$,

and the second moment of the single-particle frequencies

$$\langle B^2\rangle = \frac{1}{L}\sum_{k=1}^{L} B_k^2. \tag{14}$$

The ballistic velocity is therefore

$$v_b = J_0\sqrt{\frac{2L\langle B^2\rangle\zeta(2\nu)}{9}}. \tag{15}$$

For our particular choice for the single-particle frequencies, $B_k = B_0+\delta B_k$, where δB_k is a small random shift in the interval $(-\delta W, \delta W)$, we can further simplify Eq. (14) as

$$\langle B^2\rangle \simeq B_0^2 + \frac{\delta W^2}{3}. \tag{16}$$

We test Eq. (13) in Fig. 2(b) for a sufficiently large system size ($L = 96$) and different interaction strengths. The collapse of the curves, indicate good agreement with that equation. In addition to strong interactions ($J_0 \geq 3$), we also include an example of moderate interaction strength ($J_0 = 1.5$) to show that, in this case, since ergodicity is not fully achieved, the energy shell is not completely filled (compare the black curve with the red one).

To summarize, the ballistic motion is described by the following relation,

$$(\Delta E_0)^2(t) = v_b^2 t^2 \qquad \text{with} \qquad v_b = v_0 J_0\sqrt{L}, \tag{17}$$

where we stress the dependence of v_b on the system size L and the interaction strength J_0. The constant

$$v_0 = \frac{1}{3}\sqrt{2\zeta(2\nu)\langle B^2\rangle} \tag{18}$$

depends only on the interaction range ν and on the second moment $\langle B^2\rangle$ of the single-particle frequencies. For our choices of parameters, $v_0 \simeq 0.53$.

In what follows, we use v_b to find the ballistic time τ_b at which the ballistic regime ends and the diffusion process starts, provided that chaos is strong. To estimate τ_b, we also need the analytical dependence of the diffusion coefficient D on the model parameters, which is the subject of the next subsection. It is interesting to see how the dependence of v_b and D on L combine to guarantee that τ_b is independent of system size. Furthermore, as we will see in Sec. III C, the diffusion time τ_d also turns out to be independent of L.

B. Diffusive regime

As seen in Fig. 1(b), the variance of the single-particles energies after $t \approx \tau_b$ grows linearly in time when the interaction is strong, which allows us to write a "diffusion-like" relation,

$$(\Delta E_0)^2(t) \simeq Dt, \tag{19}$$

and associate D with a diffusion coefficient. In Fig. 3 we use quantum number $S = 2$ and show the time dependence of $(\Delta E_0)^2(t)$ for a fixed system size L varying the interaction strength J_0 [Fig. 3(a)] and for a fixed strong interaction J_0 varying the system size L [Fig. 3(b)].

In Fig. 3(a), the system size is relatively small ($L = 6$) to make possible the comparison with the quantum dynamics. We deduce from this figure that the slope of the linear growth is proportional to the interaction strength, so $D \propto J_0$. By rescaling the variance to the system size, we observe in Fig. 3(b) that the curves for large values of L are superimposed. This indicates that for large system sizes, we also have $D \propto L$, while for small L, finite-size effects are relevant. Combining these results one gets the dependence

$$D = c_0 J_0 L, \tag{20}$$

where $c_0 \approx 0.2$ is a constant obtained with a linear fitting. We stress that the diffusion-like spreading in the energy shell is independent of the choice of parameters, provided they ensure strong quantum chaos. The underlying mechanism of this diffusion-like dynamics may have a similar origin to that of the celebrated kicked rotator model, which is a 1D time-dependent system [32]. In this model, quantum diffusion, characterized by the linear increase in time of the second moment of the energy, follows closely the classical diffusion up to a certain time. Nevertheless, while classical diffusion is irreversible [33] due to local exponential instability associated with the classical dynamics, quantum diffusion is reversible, due to the linearity of Schrödinger equation. It is an open question whether a picture similar to the one developed for the kicked rotator could be extended to our many-dimensional system.

Equating Eq. (17) and Eq. (19),

$$(\Delta E_0)^2 = v_b^2\tau_b^2 = D\tau_b,$$

and using Eq. (20), we can get an estimate for the time τ_b at which the diffusion starts,

$$\tau_b = \frac{c_0}{J_0 v_0^2} = \frac{9c_0}{2\zeta^2(2\nu)}\frac{1}{J_0\langle B^2\rangle}, \tag{21}$$

where the latter equality is obtained by substituting the value of v_0 given in Eq. (18). This estimate indicates that the time at which diffusion starts is independent of L and is inversely proportional to the interaction strength J_0. While it is understandable that the diffusion process should start earlier if one increases the inter-particle interaction, the independence of τ_b on the system size L might seem unexpected at a first sight. As we show in the next section, this is not a peculiarity of our model, but should be a common feature of spin systems.

Our results are numerically confirmed in Fig. 2. In Fig. 2(a), where the interaction strength is large and different values of L are considered, we mark the intersection between the lines that give the ballistic and the diffusive behaviors. As indicated with a vertical solid, these crossing points and therefore τ_b are independent of the system size L. On the other hand, in Fig. 2(b), where a large system size ($L = 96$) and different interaction strengths are considered, one sees that τ_b depends on J_0. In this panel, the energy spreading is shown as a function

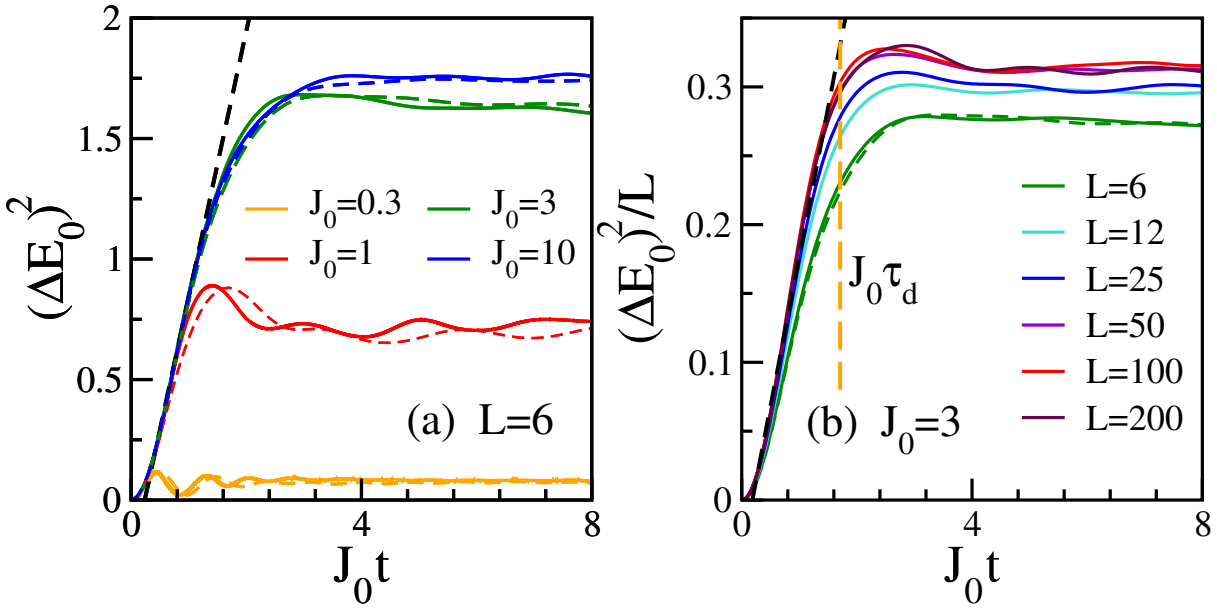

FIG. 3. (a) Energy spread $(\Delta E_0)^2$ as a function of the renormalized time J_0t for a fixed number of spins, $L = 6$, and different interaction strengths J_0, and (b) renormalized energy spread *vs* J_0t for a fixed interaction strength, $J_0 = 3$, and different system sizes L. Quantum (dashed lines) and classical (solid lines) are shown. The black dashed line in both panels indicates the linear (diffusive) growth with slope given by the fitted diffusion coefficient D in Eq. (20) for $J_0 = 10$ in (a) and $L = 200$ in (b). The vertical dashed line in (b) marks the diffusion timescale τ_d. For the classical case, we average over $10^4/L$ initial conditions with $|E_0| < 0.01$. For the quantum case, we average over 50 initial basis states with energy $|E_0| < 0.01$, and $S = 2$.

of the renormalized time J_0t. The fact that all curves collapse into a single one, so that one can draw a single line for the ballistic behavior and a single line for the diffusive behavior, indicates that $J_0\tau_b$ is a constant, so $\tau_b \propto 1/J_0$. The analytical expression for τ_b in Eq. (21) is shown in Figs. 2(a)-(b) as a vertical red line.

To estimate at which time the diffusion stops and equilibration sets in, we first need to estimate the saturation value. In the next subsection, we find an approximate expression for the saturation value as a function of the interaction strength J_0.

C. Relaxation to the steady state

In Ref. [19], we showed that for a sufficiently large interaction strength, $J_0 \gtrsim 3$, and a sufficiently large number of spins, $L > 50$, the classical motion of each single spin in the unit sphere is ergodic. We now use this result to compute the maximal energy spreading in the energy shell due to ergodicity.

Under complete ergodicity, S_k^z can be thought as a random independent variable with $\overline{S_k^z(t)} = 0$ and $\overline{S_k^z(t)^2} = 1/3$. Using this result in the definition of the energy for non-interacting spins,

$$E_0(t) = \sum_{k=1}^{L} B_k S_k^z(t), \tag{22}$$

we obtain the maximal classical energy spreading,

$$(\Delta E_0)^2_{\rm erg} = \overline{E_0^2(t)} - \overline{E_0(t)}^2 = \sum_k B_k^2 \overline{S_k^z(t)^2} = \frac{1}{3} L \langle B^2 \rangle \tag{23}$$

where we set $\overline{S_k^z(t) S_j^z(t)} = 0$ for $k \neq j$. We can further approximate this expression using Eq. (16),

$$(\Delta E_0)^2_{\rm erg} = \frac{L}{3}\left(1 + \frac{\delta W^2}{3}\right). \tag{24}$$

This is the energy spreading for completely random variables, as in the case of fully ergodic motion. Inserting our parameters $B_0 = 1$ and $\delta W = 0.2$, we obtain that

$$\Delta E_{rms} \equiv \sqrt{(\Delta E_0)^2_{\rm erg}} \simeq 0.58\sqrt{L}.$$

Notice that the width of the ergodic spreading of energy, which is $\propto \sqrt{L}$, is much smaller than the range of possible values obtained for $E_0(t)$, which is $[-\sum_k B_k, \sum_k B_k]$ and thus proportional to L.

In Fig. 4, we compare the numerical results obtained for the stationary value

$$(\Delta E_0)^2_{stat} = \lim_{T\to\infty} \frac{1}{T} \int_0^T dt\ (\Delta E_0(t))^2 \tag{25}$$

with the analytical result in Eq. (23) as a function of J_0. The saturation value of the energy spreading agrees with the analytical calculation for the ergodic spin motion when $J_0 \gtrsim 3$, thus confirming once more the ergodicity of the motion for strong interaction. For smaller

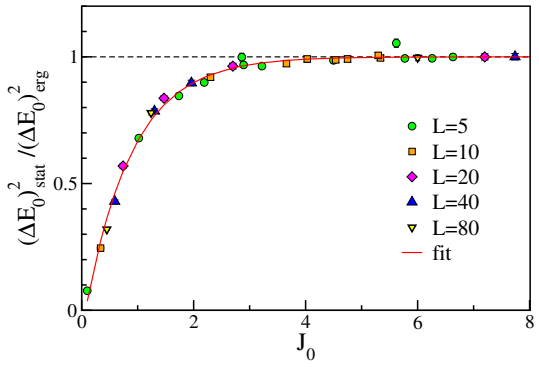

FIG. 4. Stationary classical energy spreading (symbols) compared with the ergodic energy spreading in the energy shell (horizontal dashed line) as a function of the interaction J_0 for different system sizes L. The horizontal dashed line stands for the ergodic spreading $(\Delta E_0)^2_{stat} = (\Delta E_0)^2_{\rm erg}$ as given in Eq. (24). The red curve is the fitting with the function $f(x) = 1 - ae^{-bx}$, where $a = 1.09$ and $b = 1.19$ are the best fitting parameters.

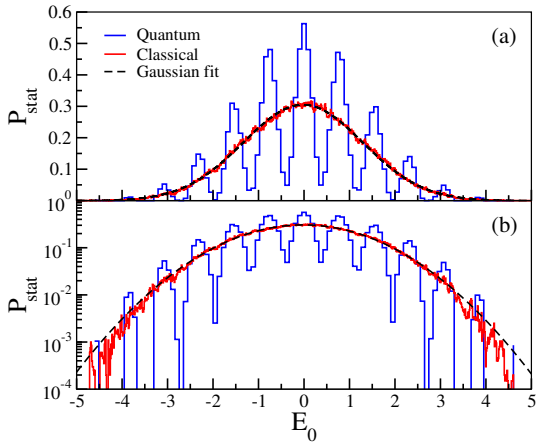

FIG. 5. Comparison between classical and quantum stationary distributions of the non-interaction energy for $L = 6, J_0 = 3$. The initial states are the same as those reported in Fig.1. Spin quantum number $S = 2$. Panel (a) is in normal scale, while (b) is in semi-log scale to show the Gaussian envelope.

values of the interaction strength, when the motion is not fully ergodic, we achieve an approximate expression for the saturating value of the energy spreading by fitting our data with a two-parameters function, $f(J_0) = 1 - ae^{-bJ_0}$, which gives

$$(\Delta E_0)^2_{stat} = (1 - ae^{-bJ_0})(\Delta E_0)^2_{\rm erg}. \qquad (26)$$

The above equation is accurate for all J_0 values, as shown with the red curve in Fig. 4. The fitting function is compatible with the fact that there is no energy spreading in the absence of interaction ($J_0 = 0$).

Now we have the necessary ingredients to estimate the relaxation time, τ_d, for the energy spreading from the relation

$$D\tau_d = (\Delta E_0)^2_{stat}.$$

In the case of the fully ergodic motion, we can substitute $(\Delta E_0)^2_{stat}$ with the analytical expression in Eq. (24), $(\Delta E_0)^2_{\rm erg}$, leading to

$$\tau_d = \frac{\sum_{k=1}^{L} B_k^2}{c_0 L J_0} = \frac{\langle B^2 \rangle}{3c_0 J_0}, \qquad (27)$$

This estimate shows that the relaxation time for the energy spreading is independent of the system size, which is numerically confirmed in Fig. 3(b).

To close this section, let us remark that the linear behavior of the quantum spreading cannot be treated as the fingerprint of "true" diffusion in the energy shell and this is why we refer to Eq. (19) as "diffusion-like" behavior. Indeed, a close inspection in Fig. 5 of the stationary energy distribution shows that it is Gaussian for the classical case, but not for the quantum model, where there are $2LS + 1$ peaks enveloped by the Gaussian distribution.

Due to the finite size of the energy shell, the variance $(\Delta E_0)^2(t)$ for time $t \gg \tau_d$ saturates. For a real diffusive process, we expect the stationary energy distribution to become Gaussian. This is indeed what happens for the classical model, as seen in Fig. 5, with the exception of the far tails [Fig. 5(b)]. The quantum distribution, on the other hand, exhibits a clear band structure, as seen in Fig. 5. The absence of a Gaussian shape prevents the association with "true" diffusion, even though $(\Delta E_0)^2$ spreads linearly in the quantum domain. Yet, since there are $2LS+1$ bands and the total size of the energy shell is $\sim 2L$, the quantum distribution approaches the classical one in the semiclassical limit, $S \gg 1$ at fixed L.

To summarize the results of this section up to now, we have found that there are two timescales, one at which the diffusive behavior starts and the other where it ends. Both times are proportional to $1/J_0$, which is physically understandable, and both are independent of the number of spins L.

D. Local instability: The Lyapunov timescale

Since the single-particle energy spreading occurs in a diffusive-like manner, one could expect it to be governed by local instabilities of the motion. Instability is the main mechanism for diffusion, because it is associated with random trajectories and chaos.

Motivated by the role of the Lyapunov timescale, τ_λ, in chaotic systems [28, 34–38], we investigate whether this timescale plays any role in the description of the relaxation to equilibrium of $(\Delta E_0)^2(t)$. Despite the link between chaos and diffusion, these two timescales, τ_λ and τ_d, do not need to be necessarily equal.

Even though the many-body system is characterized by the spectrum of all Lyapunov exponents (see [19]), the maximal exponent sets the smallest time scale for instability. For this reason, we study the maximal Lya-

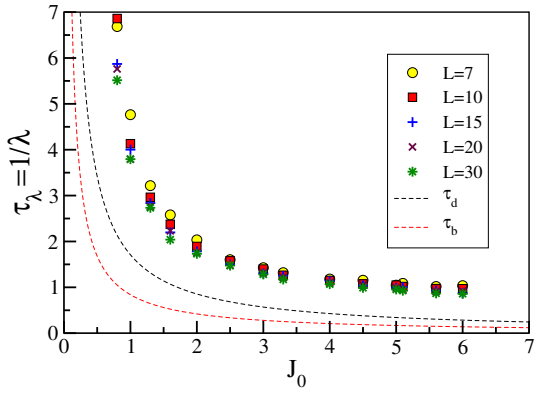

FIG. 6. Comparison between the inverse of the maximal Lyapunov exponent (Lyapunov time) for various system sizes L and the timescales for ballistic, τ_b [Eq. (21)], and diffusive, τ_d [Eq. (27)], energy spreading as a function of the interaction strength J_0.

punov $\lambda_{\max}$ exponent averaged over many different initial conditions with the same single-particle energy $E_0 = 0$. We stress that even though the maximal Lyapunov exponent decreases as the interaction strength decreases, it remains nonzero for weak interaction, $J_0 < 1$. It is only at the integrable limit, $J_0 = 0$, that $\lambda_{max} = 0$. For weak interaction, there is absence of classical ergodicity, but the model is still chaotic [19].

In Fig. 6 we plot the Lyapunov time, which is the inverse of the Lyapunov exponent, $\tau_\lambda = 1/\lambda_{max}$, as a function of the interaction strength J_0 for different system sizes L. We see that τ_λ is almost independent of L for large interaction strengths, $J_0 \gtrsim 3$. The figure suggests that the behavior of the Lyapunov time τ_λ as a function of J_0 is comparable to that of τ_d in the range of interactions J_0 where diffusion is observed. The discrepancy between the two may be caused by the fact that the timescale for local instability is defined up to some constant, since it is related to the time at which the distance Δ between close trajectories becomes of the order $\Delta < 1$.

IV. LOCAL OBSERVABLE: SINGLE SPIN RELAXATION

Having established the timescales for the energy spread in the energy shell, we now move our attention to a local observable, namely, to the S_z component of an individual spin. The initial many-body state that we choose for the quantum model is

$$|\Psi(0)\rangle = |0, ..., 0, S, 0, ..., 0\rangle,$$

where only the spin $m = \lfloor L/2 \rfloor$ in the middle of the chain has maximal value S along the z-direction, while all other $L-1$ spins have zero value for the z-component. The corresponding classical initial condition is $S^z_{\lfloor L/2 \rfloor}(0) = S/\sqrt{S(S+1)}$ for the central spin, $S^z_k(0) = 0$ for the other spins, and the x, y components are randomly chosen keeping the length of the spins fixed. We investigate the time that it takes for the "excitation" on site $\lfloor L/2 \rfloor$ to get shared with the other $L-1$ spins and whether the characteristic time for the relaxation is the same τ_d as the one obtained in Eq. (27).

We show the evolution of the onsite magnetization of the central spin m for different ranges ν of the interaction in Fig. 7(a), for different system sizes in Fig. 7(b), and for different interaction strengths in Fig. 7(c). The results in Fig. 7(a) indicate that when the interaction is short range, the relaxation time does not depend on the value of ν. The excellent quantum-classical correspondence in all panels gives us access to large system sizes through the classical dynamics, as done in Fig. 7(b). This plot makes it evident that the timescale for the relaxation is independent of L. Figure 7(c) shows that the relaxation time does depend on the interaction strength, as it also does for the energy spreading.

To compare the relaxation time for the onsite magnetization with that for the energy spreading, we mark with a vertical dashed line in Figs. 7(a)-(c), the diffusion time τ_d obtained in Eq. (27) and find good numerical agreement with it. Therefore, our results presented in Fig. 3 and Fig. 7 confirm that both the local and the global quantity considered here exhibit the same relaxation timescale, independently of the length L.

To test the robustness of our results, we study the classical dynamics of a large chain by changing the frequencies of each single spin from approximately constant, $B_k \sim B_0$, to completely random inside an interval $(0, W)$. This interval is chosen to reproduce the same second moment $\langle B^2 \rangle$ as in the almost constant case, so that we can verify whether the relaxation time in the new scenario still coincides with τ_d given in Eq. (27). We compare the two cases for the global observable (energy spreading) in Fig. 8(a) and for the local observable (single spin z-component) in Fig. 8(b). In both panels, both curves (for almost constant frequencies and for random frequencies) follow the same evolution characterized by the same relaxation time. The fact that the dynamics for both observables, global and local, does not change when we change the spin frequencies can be understood from the following physical point of view. Even if initially only the S^z component of a single spin is excited, $S^z_m(0) \approx 1$, the components $S^x_k(0)$ and $S^y_k(0)$ of all other spins cannot be zero due to the spin conservation, $(S^x_k)^2 + (S^y_k)^2 + (S^z_k)^2 = 1$ (i.e. L additional constants of motion, apart from the total energy). This means that for any initial excitation, the interaction immediately excites all spins in the chain.

V. LINEAR CHAOS AND THE PARAMETRIC OSCILLATOR

Having demonstrated that the diffusion time τ_d for the global and local observables are independent of the system size L, we now provide insight into the properties of

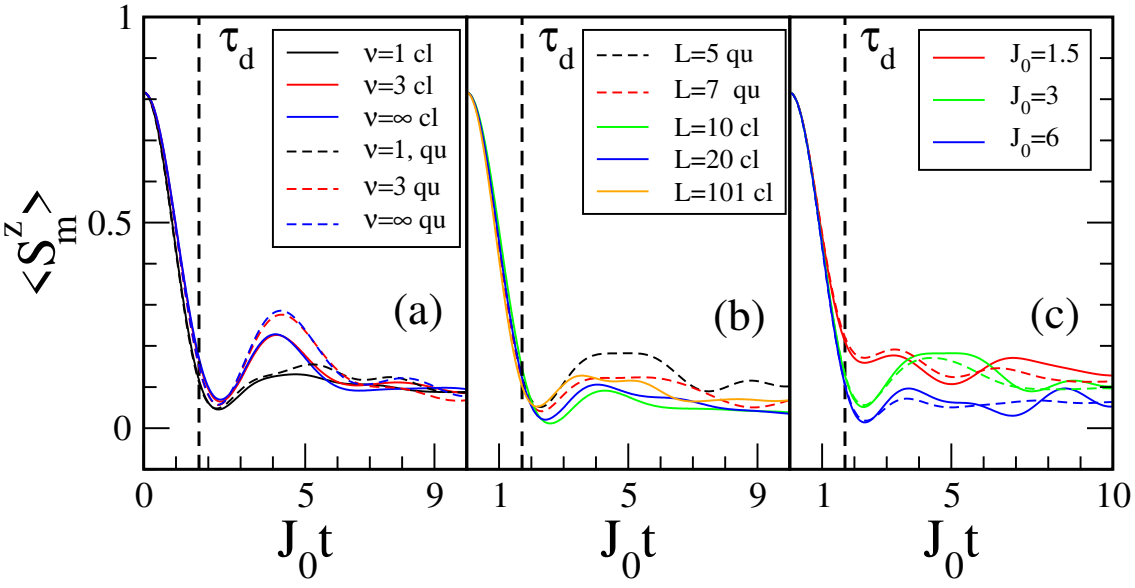

FIG. 7. Quantum (dashed curves) and classical (solid curves) evolution of the z-component of the central spin for: (a) different ranges ν of the interaction and fixed system size $L = 5$ and $J_0 = 3$; (b) different system sizes L, fixed $\nu = 1.4$ and $J_0 = 3$; (c) different interaction strengths J_0, same $L = 5$ and $\nu = 1.4$. The vertical lines stand for the diffusion timescale τ_d obtained in Eq. (27). The quantum initial state is $|\Psi(0)\rangle = |0, ..., 0, S, 0, ..., 0\rangle$. The classical initial condition corresponds to $S^z_{m=\lfloor L/2 \rfloor}(0) = S/\sqrt{S(S+1)}$ and $S^z_k(0) = 0$ for $k \neq m = \lfloor L/2 \rfloor$, and the x, y-components are chosen at random, apart from the m-th spin for which $S^x_m = S^y_m = 0$. We use $10^4/L$ classical initial conditions. For all quantum data $S = 2$.

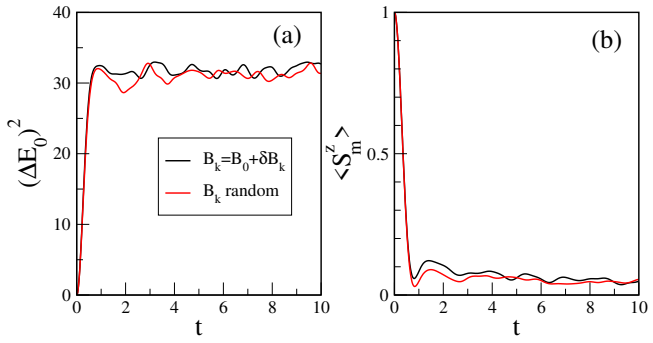

FIG. 8. Slightly random (black line) vs fully random spin-frequencies (red line). The energy spreading (a) and the evolution of the z-component of the spin in the middle of the chain, $m = \lfloor L/2 \rfloor$ (b) for the classical model. Here $L = 100$, $\nu = 1.4$, $J_0 = 3$. The average is done over 10^3 different initial conditions with $|E_0| < 0.01$.

the classical model and use them to justify those results. To do this, we concentrate on the evolution of $S^z_k(t)$, described by Eq. (7), where the time-dependent frequency $\Omega^2_k(t)$ and the driving nonlinear force $F_k(t)$ are given in Eq. (8) and depend on all other spin components.

Equation (7) describes a parametric oscillator with frequency $\Omega_k(t)$ and driving force $F_k(t)$. Notice that both terms $\Omega_k(t)$ and $F_k(t)$ do not depend explicitly on $S^z_k(t)$. Such dependence emerges only in the second order of the perturbation theory in J_0, when we take into account the dependence of the $S^{x,y}_j$-components on S^z_k. This means that for nonzero but small values of J_0, one can neglect the nonlinear effects of the coupling between the spins and can describe the time-dependence of $S^z_k(t)$ with the use of a *linear* parametric oscillator. Even if one neglects the nonlinear terms contained in Ω_k and F_k, the motion of the k-th spin can still be strongly chaotic and described by a positive Lyapunov exponent. The chaotic motion of S^z_k is due to parametric instability and not to the nonlinear effects of the spin motion. This kind of chaos was named *linear chaos* by Chirikov [39]. This behavior finds a parallel in the motion of charged particles in magnetic traps [40] and linear maps [41].

To better explain the notion of linear chaos [39], let us consider the evolution of $S^z_k(t)$ in the first order approximation in J_0 by inserting in the expressions for $\Omega_k(t)$ and $F_k(t)$ the unperturbed solutions of S^x_k, S^y_k described by linear rotations with frequency B_k. In this way, Eq. (7) for each spin describes a linear oscillator with time-dependent frequency and linear force. The instability of this oscillator can be inferred from the integration of the equations of motion. This picture still holds approximately on increasing the perturbation strength J_0 as shown in Figs. 9(a)-(b), where the results for the spin in the middle of the chain are compared with the exact full dynamics for two different system sizes L. One sees that the timescales for the relaxation of the linear parametric oscillator are effectively the same as that for the full dynamics and clearly do not depend on L.

Therefore, taking the property of linear chaos of our model into account, it becomes clear that increasing the

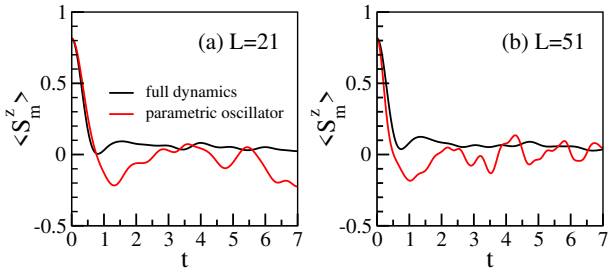

FIG. 9. Comparison between the evolution of the classical spin in the middle of the chain described by a linear parametric oscillator (red curve) and by the full dynamics (black curve) for $L = 21$ (a) and $L = 51$ (b). The classical initial condition has $S^z_m(0) = S/\sqrt{S(S+1)}$ and $S^z_k(0) = 0$ for $k \neq m = \lfloor L/2 \rfloor$, and the other components are chosen randomly. The average is done over $10^4/L$ classical initial conditions. The parameters are $J_0 = 3$, $\nu = 1.4$, $B_0 = 1$, $\delta W = 0.2$.

system size L simply implies adding more harmonics in the expression of the driving force F_k and the time-dependent frequency $\Omega_k(t)$. Since even a small number of incommensurate frequencies B_k is enough to produce effective randomness, adding more frequencies does not change much the results. This is why increasing L does not affect significantly the dynamics of single spins in their motion on the unit sphere.

VI. QUANTUM OBSERVABLE WITH NO CLASSICAL LIMIT

In the previous sections, we investigated quantities that have a classical limit. We now analyze a quantum observable that has no classical limit, namely the participation ratio,

$$P_R(t) = \frac{1}{\sum_k |\langle k|\Psi(t)\rangle|^4}. \tag{28}$$

This quantity is purely quantum, because it measures the effective number of many-body basis states $|k\rangle$ occupied by the evolved state $|\Psi(t)\rangle$ at time t. Changing the basis representation changes the value of $P_R(t)$, so no classical limit can be defined. This quantity describes global relaxation in the Hilbert space.

Knowledge of the energy distribution of the initial state, the so-called LDoS, helps with the description of the evolution of $P_R(t)$. The LDoS is defined as

$$W_{k_0}(E) = \sum_\alpha \delta(E - E_\alpha)|C^\alpha_{k_0}|^2, \tag{29}$$

where the coefficients $C^\alpha_{k_0} = \langle \alpha|k_0\rangle$, as in Eq. (5), and $|k_0\rangle$ is an initial state corresponding to a non-interacting basis state, typically taken in the middle of the energy spectrum. The width of the LDoS is given by

$$\sigma = \sum_{k\neq k_0} \langle k|H|k_0\rangle = \sum_\alpha |C^\alpha_{k_0}|^2 E^2 - \left(\sum_\alpha |C^\alpha_{k_0}|^2 E\right)^2. \tag{30}$$

When the initial state is composed of many chaotic eigenstates of the total Hamiltonian, $P_R(t)$ grows exponentially in time with a rate given by the width of the LDoS [22], as shown, for instance, in Fig. 10(a). To extract a reliable estimate for the relaxation timescale, in Fig. 10(b), we rescale $P_R(t)$ to the dimension, dim, of the subspace associated with the initial state and verify that all curves saturate at the same point. For values of J_0 that ensure quantum chaos, the saturation point of $P_R(t)$ is roughly $\dim/2 = (2S+1)^L/4$. Due to this result, we can find an analytical estimate of the timescale τ_N for the relaxation of $P_R(t)$ using the equality

$$P_R(\tau_{_N}) \simeq e^{2\sigma\tau_{_N}/\hbar} = (2S+1)^L/4, \tag{31}$$

which gives

$$\tau_{_N} \propto L\hbar \ln(2S+1)/\sigma. \tag{32}$$

In the equation above, σ is the width of the quantum LDoS written in Eq. (30)

It is difficult to obtain analytical estimates for the width of the quantum LDoS, because it requires the exact diagonalization of Hamiltonian matrices that are exponentially large in L. Nevertheless, using the quantum-classical correspondence exploited in Ref. [19], it is possible to build numerically the classical LDoS. The agreement between the classical and quantum LDoS in the quantum chaotic regime is impressive even for small spin quantum numbers $S = 1, 2$ as shown in Fig. 11. We can then use the classical LDoS to estimate the width σ_{cl} for large system sizes. This is a crucial result, because it implies that instead of the diagonalization of huge matrices, we can get information about the LDoS by simply integrating $3L$ differential equations, which can be done for systems as large as $L = 10^2$ spins with a standard laptop. This "semi-quantal" approach was discussed in [19] and also in [42].

Using the classical equations of motion, we arrive at

$$\sigma^2_{cl} = \frac{J_0^2}{9}\sum_{k=1}^{L}\sum_{j>k}\frac{1}{|j-k|^{2\nu}} \equiv \frac{J_0^2}{9}\zeta(\nu, L), \tag{33}$$

where the symbol "$\equiv$" defines implicitly the function $\zeta(\nu, L)$ for any ν and finite L. For large values of L, this function can be approximated as

$$\zeta(\nu, L) \simeq (L-1)\sum_{k=1}^{\infty}\frac{1}{k^{2\nu}} = (L-1)\zeta(2\nu), \tag{34}$$

where $\zeta(2\nu)$ is the Riemann zeta function. Thus, for sufficiently large L, we get that

$$\sigma_{cl} \simeq \frac{J_0\sqrt{L-1}\zeta(2\nu)}{3}. \tag{35}$$

This result holds for any $\nu > 1/2$, when the Riemann

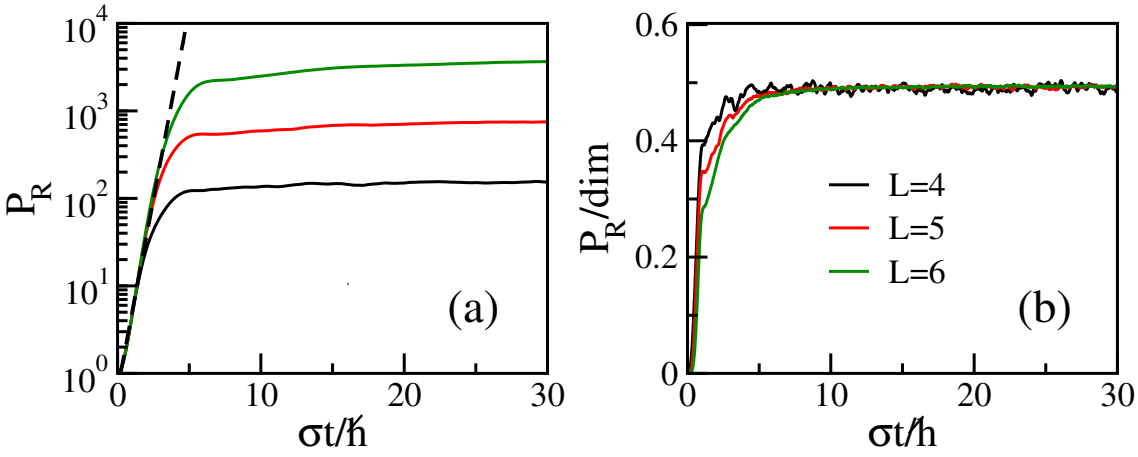

FIG. 10. (a) Participation ratio, P_R, and (b) participation ratio renormalized by the dimension of the Hilbert space as a function of time renormalized by the width of the LDoS, $\sigma t/\hbar$, for different system sizes L. The dashed line in (a) is $e^{2\sigma t/\hbar}$. The average is performed over 50 initial states in the energy range $|E| < 0.01$, $J_0 = 3$, $S = 2$.

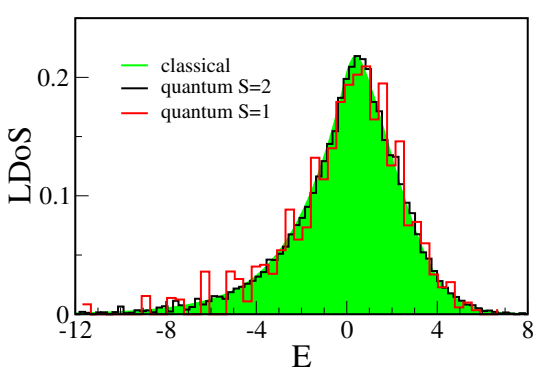

FIG. 11. Quantum and classical LDoS for $L = 6$, $J_0 = 3$. The histograms for the quantum case are for spin number $S = 1$ (red) and $S = 2$ (black). The shaded histogram represents the classical LDoS.

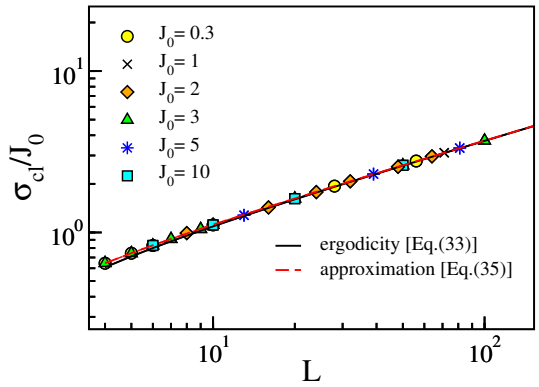

FIG. 12. Classical width of the LDoS divided by the interaction strength, σ_{cl}/J_0, as a function of the system size L. Full (black) line is the ergodic approximation for finite L in Eq. (33) and the red dashed curve stands for the expression for the ergodic approximation for large L in Eq. (35).

zeta function converges.

In Fig. 12, we compare numerical results for the classical width of the LDoS with the exact expression for finite L in Eq. (33) and with the approximate expression in Eq. (35). As one can see, even for $L \gtrsim 10$, the approximate expression matches extremely well the numerical data.

Using the analytical result for the classical width of the LDoS in Eq. (35), we finally get the estimate for the relaxation time for $P_R(t)$,

$$\tau_{_N} \propto \sqrt{L}\frac{1}{J_0}\frac{\ln(2S+1)}{\sqrt{S(S+1)}}. \tag{36}$$

The above equation indicates that for any fixed S, the relaxation time grows with L, as indeed noticeable in Fig. 10(a). On the other hand, for a fixed L, Eq. (36) indicates that $\tau_{_N}$ slowly decreases as S increases (see also [43]). This means that for $P_R(t)$, the thermodynamic and the semiclassical limit of Eq. (32) lead to opposite conclusions, a result that requires further analysis.

VII. CONCLUSION

We explored the quantum-classical correspondence (QCC) of many-body spin systems to investigate their relaxation dynamics after a quench. In the regime of strong chaos, we verified that the quantum and classical dynamics are analogous even for spins as small as $S = 1, 2$. The QCC allows for the use of the classical system to compute the timescales of very large quantum systems. This is what we did to derive semi-analytical results for the timescales governing the spread of the single-

particles energies, $(\Delta E_0)^2(t)$, and the relaxation of the z-magnetization of individual spins, $\langle S_k^z(t)\rangle$.

The analysis of $(\Delta E_0)^2(t)$ revealed three distinct time regions. The first one, arising from perturbation theory, corresponds to the ballistic spread of energy up to τ_b. Subsequently, the energy spread exhibits a diffusive-like behavior that persists until τ_d, when the dynamics saturates due to the finite width of the energy shell. Supported by the results in Ref. [19], where we showed that for strong interaction the classical motion of each spin is ergodic in its unit sphere, we verified that both the ballistic and diffusion timescales are independent of the system size L.

The fact that diffusion is conditioned to the existence of chaos prompted the question of how the Lyapunov timescale, τ_λ, measured as the inverse value of the Lyapunov exponent, compares with the diffusion time τ_d. The Lyapunov time characterizes the local instability of the motion of individual spins, while the diffusion time determines the global energy spread in the energy shell, so, in principle, there is no reason why the two timescales should coincide. Yet, our numerical data revealed that τ_λ is of the same order as τ_d, and once again does not depend on the system size.

Our analysis of the classical and quantum evolution of $\langle S_k^z(t)\rangle$ demonstrates that the relaxation time for this local quantity, just as for the global quantity $(\Delta E_0)^2(t)$, does not depend on L either. We expect this result to be general and confirmed for other physical observables with a well-defined classical limit.

We found that the diffusion time depends on the single-particle frequencies B_k and the interaction strength J_0 as $\tau_d \propto \langle B^2\rangle/J_0$. We showed that the lack of dependence of this timescale on system size is robust whether the frequencies are nearly constant or completely random. Nevertheless, the expression for τ_d naturally raises the question of whether one could engineer the frequencies to induce a system-size dependence on the relaxation process. This would provide a tool to control the properties of the dynamics.

A closer look at the classical equations of motion allowed us to better justify why the relaxation time of $\langle S_k^z(t)\rangle$ does not depend on system size. The second-order differential equation for S_k^z describes a parametric oscillator. The nonlinearities contained in the time-dependent frequency and force of the oscillator are small and are not significantly affected by the system-size increase. Indeed, our results show that neglecting the nonlinearities lead to a similar relaxation time as that of the full dynamics, independently of L.

Motivated by various studies [18, 21, 22, 29] of the relaxation process of the participation ratio, $P_R(t)$, we also analyzed this quantity despite its lack of a classical limit. As demonstrated analytically and verified numerically, in the region of strong quantum chaos, $P_R(t)$ grows exponentially before reaching saturation. The exponential growth is governed by the width of the Local Density of States (LDoS). As explained in [19], this width can be obtained from the classical counterpart of the model, which gives us access to large system sizes. We find that the relaxation of the participation ratio is proportional to $\sqrt{L}$. This implies that this quantity does not thermalize in the thermodynamic limit, $L \to \infty$. This outcome stresses the significance of the chosen quantity in defining the timescales for thermalization. It may also provide an explanation for the conflicting results for the relaxation times found in the literature, where different L-dependences are reported for quantities such as survival probability and the participation ratio.

ACKNOWLEDGMENTS

F.B. acknowledges support by the Iniziativa Specifica INFN-DynSysMath and MIUR within the Project No. PRIN 20172H2SC4. F.M.I. acknowledges financial support from CONACyT (Grant No. 286633). L.F.S. was supported by NSF Grant No. DMR-1936006. This research was supported in part by grants NSF PHY-1748958 and PHY-2309135 to the Kavli Institute for Theoretical Physics (KITP). F.M.I. and L.F.S. gratefully acknowledge support from the Simons Center for Geometry and Physics, Stony Brook University at which some of the research for this paper was performed.

[1] S. Goldstein, T. Hara, and H. Tasaki, Time scales in the approach to equilibrium of macroscopic quantum systems, Phys. Rev. Lett. **111**, 140401 (2013).
[2] S. Goldstein, T. Hara, and H. Tasaki, Extremely quick thermalization in a macroscopic quantum system for a typical nonequilibrium subspace, New J. Phys. **17**, 045002 (2015).
[3] T. R. de Oliveira, C. Charalambous, D. Jonathan, M. Lewenstein, and A. Riera, Equilibration time scales in closed many-body quantum systems, New J. Phys. **20**, 033032 (2018).
[4] G. D. Carvalho, L. F. dos Prazeres, P. S. Correia, and T. R. de Oliveira, Equilibration of isolated systems: investigating the role of coarse-graining on the initial state magnetization (2023), arXiv:2305.11985 [quant-ph].
[5] M. Niknam, L. F. Santos, and D. G. Cory, Experimental detection of the correlation Rényi entropy in the central spin model, Phys. Rev. Lett. **127**, 080401 (2021).
[6] P. Reimann, Foundation of statistical mechanics under experimentally realistic conditions, Phys. Rev. Lett. **101**, 190403 (2008).
[7] P. Reimann, Typical fast thermalization processes in closed many-body systems, Nat. Comm. **7**, 10821 (2016).
[8] A. J. Short, Equilibration of quantum systems and sub-

systems, New J. Phys. **13**, 053009 (2011).
[9] A. J. Short and T. C. Farrelly, Quantum equilibration in finite time, New J. Phys. **14**, 013063 (2012).
[10] T. Monnai, Generic evaluation of relaxation time for quantum many-body systems: Analysis of the system size dependence, J. Phys. Soc. Jpn. **82**, 044006 (2013).
[11] A. S. L. Malabarba, L. P. García-Pintos, N. Linden, T. C. Farrelly, and A. J. Short, Quantum systems equilibrate rapidly for most observables, Phys. Rev. E **90**, 012121 (2014).
[12] D. Hetterich, M. Fuchs, and B. Trauzettel, Equilibration in closed quantum systems: Application to spin qubits, Phys. Rev. B **92**, 155314 (2015).
[13] C. Gogolin and J. Eisert, Equilibration, thermalization, and the emergence of statistical mechanics in closed quantum systems, Rep. Prog. Phys. **79**, 056001 (2016).
[14] L. P. García-Pintos, N. Linden, A. S. L. Malabarba, A. J. Short, and A. Winter, Equilibration time scales of physically relevant observables, Phys. Rev. X **7**, 031027 (2017).
[15] M. Schiulaz, E. J. Torres-Herrera, and L. F. Santos, Thouless and relaxation time scales in many-body quantum systems, Phys. Rev. B **99**, 174313 (2019).
[16] B. Bertini, F. Heidrich-Meisner, C. Karrasch, T. Prosen, R. Steinigeweg, and M. Žnidarič, Finite-temperature transport in one-dimensional quantum lattice models, Rev. Mod. Phys. **93**, 025003 (2021).
[17] A. Dymarsky, Bound on eigenstate thermalization from transport, Phys. Rev. Lett. **128**, 190601 (2022).
[18] T. L. M. Lezama, E. J. Torres-Herrera, F. Pérez-Bernal, Y. Bar Lev, and L. F. Santos, Equilibration time in many-body quantum systems, Phys. Rev. B **104**, 085117 (2021).
[19] L. Benet, F. Borgonovi, F. M. Izrailev, and L. F. Santos, Quantum-classical correspondence of strongly chaotic many-body spin models, Phys. Rev. B **107**, 155143 (2023).
[20] V. Zelevinsky, B. A. Brown, N. Frazier, and M. Horoi, The nuclear shell model as a testing ground for many-body quantum chaos, Phys. Rep. **276**, 85 (1996).
[21] F. Borgonovi, F. M. Izrailev, and L. F. Santos, Exponentially fast dynamics of chaotic many-body systems, Phys. Rev. E **99**, 010101 (R) (2019).
[22] F. Borgonovi, F. M. Izrailev, and L. F. Santos, Timescales in the quench dynamics of many-body quantum systems: Participation ratio versus out-of-time ordered correlator, Phys. Rev. E **99**, 052143 (2019).
[23] J. Rammensee, J. D. Urbina, and K. Richter, Many-body quantum interference and the saturation of out-of-time-order correlators, Phys. Rev. Lett. **121**, 124101 (2018).
[24] Q. Hummel, B. Geiger, J. D. Urbina, and K. Richter, Reversible quantum information spreading in many-body systems near criticality, Phys. Rev. Lett. **123**, 160401 (2019).
[25] M. Akila, D. Waltner, B. Gutkin, P. Braun, and T. Guhr, Semiclassical identification of periodic orbits in a quantum many-body system, Phys. Rev. Lett. **118**, 164101 (2017).
[26] M. Akila, B. Gutkin, P. Braun, D. Waltner, and T. Guhr, Semiclassical prediction of large spectral fluctuations in interacting kicked spin chains, Ann. Phys. (New York) **389**, 250 (2018).
[27] D. Schubert, J. Richter, F. Jin, K. Michielsen, H. De Raedt, and R. Steinigeweg, Quantum versus classical dynamics in spin models: Chains, ladders, and square lattices, Phys. Rev. B **104**, 054415 (2021).
[28] L. Correale, A. Polkovnikov, M. Schirò, and A. Silva, Probing chaos in the spherical p-spin glass model, SciPost Phys. **15**, 190 (2023).
[29] F. Borgonovi, F. M. Izrailev, L. F. Santos, and V. G. Zelevinsky, Quantum chaos and thermalization in isolated systems of interacting particles, Phys. Rep. **626**, 1 (2016).
[30] N. Defenu, A. Lerose, and S. Pappalardi, Out-of-equilibrium dynamics of quantum many-body systems with long-range interactions (2023), arXiv:2307.04802 [cond-mat.quant-gas].
[31] On the other hand, the question of whether the Kolmogorov-Sinai entropy (sum of positive Lyapunov exponents) has any relation with the global dynamical properties of spin models remains open, in our opinion.
[32] G. Casati, B. V. Chirikov, F. M. Izrailev, and J. Ford, Stochastic behavior of a quantum pendulum under a periodic perturbation, Lect. Notes in Phys. **9399**, 334 (1979).
[33] B. V. Chirikov, F. M. Izrailev, and D. L. Shepelyansky, Dynamical stochasticity in classical and quantum mechanics, Sov. Sci. Rev. C **2**, 209 (1981).
[34] J. Steinberg and B. Swingle, Thermalization and chaos in QED_3, Phys. Rev. D **99**, 076007 (2019).
[35] M. Malishava and S. Flach, Thermalization dynamics of macroscopic weakly nonintegrable maps, Chaos **32**, 063113 (2022).
[36] M. Malishava and S. Flach, Lyapunov spectrum scaling for classical many-body dynamics close to integrability, Phys. Rev. Lett. **128**, 134102 (2022).
[37] Z. Wang, Y. Wang, and B. Wu, Quantum chaos and physical distance between quantum states, Phys. Rev. E **103**, 042209 (2021).
[38] T. Bilitewski, S. Bhattacharjee, and R. Moessner, Classical many-body chaos with and without quasiparticles, Phys. Rev. B **103**, 174302 (2021).
[39] B. Chirikov, Linear and nonlinear dynamical chaos, Open Systems & Information Dynamics **4**, 241 (1997).
[40] B. V. Chirikov, Resonance processes in magnetic traps, The Soviet Journal of Atomic Energy **6**, 464 (1960).
[41] F. Izrailev, Nearly linear mappings and their applications, Physica D **1**, 243 (1980).
[42] F. Borgonovi, G. Celardo, F. M. Izrailev, and G. Casati, A semiquantal approach to finite systems of interacting particles, Phys. Rev. Lett. **88**, 54101 (2002).
[43] Y. Lebel, L. F. Santos, and Y. B. Lev, Chaos enhancement in large-spin chains, SciPost Phys. **15**, 022 (2023).